Natalia Strawa[1], Paweł Malczyk [1]

Modeling and control of a simplified high-speed vehicle moving in reduced-pressure conditions

In times of rapidly progressing globalization, the possibility of fast long-distance travel between high traffic cities has become an extremely important issue. Currently, available transportation systems have numerous limitations, therefore, the idea of a high-speed transportation system moving in reduced-pressure conditions has emerged recently. This paper presents an approach to the modelling and simulation of the dynamic behaviour of a simplified high-speed vehicle that hovers over the track as a magnetically levitated system. The developed model is used for control system design. The purpose of passive and active suspension discussed in the text is to improve both the performance and stability of the vehicle as well as ride comfort of passengers travelling in a compartment. Comparative numerical studies are performed and the results of the simulations are reported in the paper with the intent to demonstrate the benefits of the approach employed here.

1. Introduction

Rapid development in economics and technology, resulting in a globalization process, has heightened the need for a fast, reliable transportation system between high-traffic cities. Existing solutions, i.e., road, rail, air, and maritime transport, possess significant disadvantages which could be potentially overcome by a high-speed transportation system moving in reduced-pressure conditions – the Hyperloop system [1]. Hyperloop capsules are considered in two versions: passenger and cargo systems, which may vary in dimensions and internal equipment. A vehicle moves inside low-pressure tubes using magnetic levitation [1]. In order to decrease energy

✉ Natalia Strawa, email: strawa.natalia@gmail.com

[1]Institute of Aeronautics and Applied Mechanics, Faculty of Power and Aeronautical Engineering, Warsaw University of Technology, Warsaw, Poland. Emails: strawa.natalia@gmail.com, pmalczyk@meil.pw.edu.pl

consumption, a passive Inductrack levitation system is implemented [2, 3]. This is an alternative solution to Maglev trains, where many active systems are used simultaneously [1, 4].

In this paper, we investigate the stability and dynamic performance of a preliminary design of a vehicle with different suspension variants. The concept of this work comes from the research and development activities conducted at the Warsaw University of Technology for the last few years. The dynamic response of a system is extremely important in several practical aspects: safety and ride quality, guideway design, and system costs [5, 6]. Track roughness may induce random vibrations which are perceived by passengers in the vehicle. Vibrations can cause many physiological effects; hence, ride quality is a serious constraint in suspension system design. Ride comfort can be enhanced by introducing a control scheme into the suspension design.

In recent years, extensive research into the active and semi-active suspension systems of automotive vehicles has been conducted [7]. A variety of control approaches can be found in the literature. Usually, authors conduct their research on a quarter-suspension model which significantly simplifies the analysis while providing the results easily transferable to the full vehicle model. In [8–10], classical methods such as PID controller were proposed. Some authors, on the other hand, investigate the performance of the more complex techniques, such as optimal control methods [11] or sliding mode control [12]. In [5] and [13], suspension control is implemented on the high-speed Maglev train.

In our study, we also propose a control system design for a magnetic suspension, however, unlike in [5, 13], our study focuses on a passive electrodynamic levitation system, which introduces an element of novelty into our research. This study identifies the basic stability characteristics of the system through the use of simplified models that capture various phenomena important in the determination of ride quality and vehicle stability. The multiloop control system for a quarter-suspension model is proposed in this paper aiming at increasing passengers' ride comfort. The theory and simulation-based results are collected for a planar three degree of freedom vehicle, which is composed of two one-dimensional suspension modules (i.e., quarter-suspension systems). Conclusions and future research plans are also addressed at the very end of the paper.

2. Simplified vehicle model

2.1. Quarter-suspension model

For control system design purposes, it is desirable to consider low-order linear dynamic models [5]. Thus, a two-degree-of-freedom quarter-suspension model has been selected for the analysis. The developed low-order model consists of a primary and secondary suspension. As a result, only the vertical motion of the vehicle is considered. Still, such simplified analysis is sufficient and of very practical value in

terms of vehicle dynamics and ride comfort examination [5, 14]. Moreover, such a linear time-invariant system allows one to use a variety of control design techniques for this kind of system.

The simplified model used in control synthesis is presented in Fig. 1. Quarter-suspension consists of two lumped masses m_p and m_s, which together equal 1/4 of the vehicle body mass, one linear spring k_s, one viscous damper b_s, and one Halbach array [2], employed as a magnetic levitation system. The forces induced in the magnets are non-linear functions of vehicle longitudinal velocity and levitation height, however, it can be proved that for high speeds, the force is constant with respect to velocity. Therefore, by linearizing the magnetic lift about the equilibrium condition at which the suspension is at a levitation height, the magnetic force can be modelled as a linear spring (spring constant k_m^*). The quantities with subscripts p and s refer to primary and secondary suspension systems, respectively. The symbols z_p and z_s are used to define the position of lumped masses with respect to their equilibrium positions, respectively. The z_t symbol describes a disturbance induced from track irregularity.
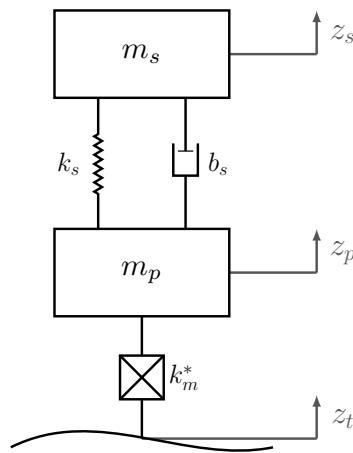

Fig. 1. One-dimensional 2 DOF quarter-suspension model of a vehicle

Some advantages of such model simplifications can be pointed out. Firstly, the basic concept of a suspension system can be easily grasped. Secondly, the developed model allows one to capture the essential behaviour of the system. The coupling effects of primary and secondary suspension, which may affect ride comfort significantly [5], are not ignored in the model. Last but not least, the model is similar to some extent to the developments used in the examination of dynamics and control of Maglev vehicles [5]. This feature may partially confirm the validity of the approach proposed in the paper. It should be pointed out that the official literature on Hyperloop vehicle dynamic performance is very modest so far.

It is assumed in this paper that a Hyperloop suspension system may levitate over a track equipped with Halbach arrays provided that the critical speed is achieved. The magnetic levitation force induced in the system (i.e., between a track and a vehicle) can be divided into two components: lift and drag forces. The quantities can be represented by the following expressions [2]:

$$F_L(V, h) = \Lambda_L \frac{V^2}{V^2 + \beta^2} e^{-\alpha h} \quad \text{[N]}, \tag{1a}$$

$$F_D(V, h) = \Lambda_D \frac{V}{V^2 + \beta^2} e^{-\alpha h} \quad \text{[N]}, \tag{1b}$$

where Λ_L, Λ_D, α, β are constant values dependent on the levitation system geometric and magnetic properties such as Halbach array dimensions, number of magnets in the array, remanent field of the magnets, etc., h is an air-gap between the magnets and the track (levitation height), and V is a longitudinal velocity of a system. The levitation system parameter values used in this study are provided in Table 1.

Table 1.

Levitation system parameters

Parameter	Value	Unit
Λ_L	3.0712×10^5	$\text{T}^2\text{m}^3/\text{H}$
Λ_D	16.5620×10^5	$\text{T}^2\text{m}^4\Omega/\text{H}^2$
α	104.7199	1/m
β	5.3927	$\Omega\text{m}/\text{H}$

It can be observed that both lift and drag forces decay with an increasing air gap. For small air gap values, a decrease in lift and drag force is rapid and approaches zero when the levitation height increases. The graphical representation of this relation is presented in Fig. 2.

On the other hand, a linear velocity increase saturates the lift force but causes a sharp decrease of the drag force, which is undoubtedly an advantage of Inductrack magnetic levitation. Fig. 3 provides the profile of forces F_L and F_D in terms of velocity at constant levitation height at several different air gaps.

Closer inspection of the graphs can lead to the conclusion that passive levitation is the most efficient process at high operating speeds when the lift force reaches its asymptotic maximum value for a given air gap, while drag remains significantly smaller at the same time.

The lift force (1a) is a nonlinear quantity. One can linearize the expression about the operating point: travel velocity and equilibrium (levitation) height:

$$\widetilde{F_L}(V, h) \cong \widetilde{F_L}(V_0, h_0) + \frac{\partial \widetilde{F_L}(V_0, h_0)}{\partial V} \Delta V + \frac{\partial \widetilde{F_L}(V_0, h_0)}{\partial h} \Delta h. \tag{2}$$
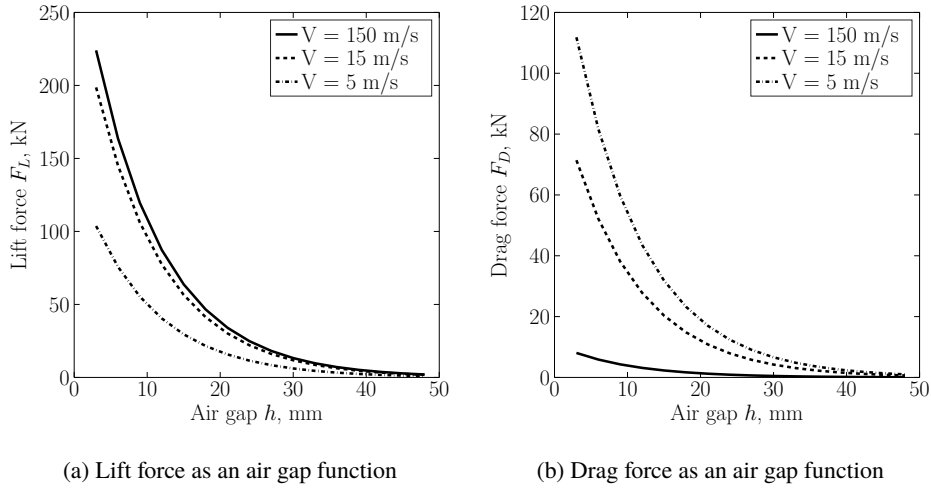
(a) Lift force as an air gap function

(b) Drag force as an air gap function

Fig. 2. Lift (a) and drag (b) forces as an air gap function for constant velocity values

(a) Lift force as velocity function
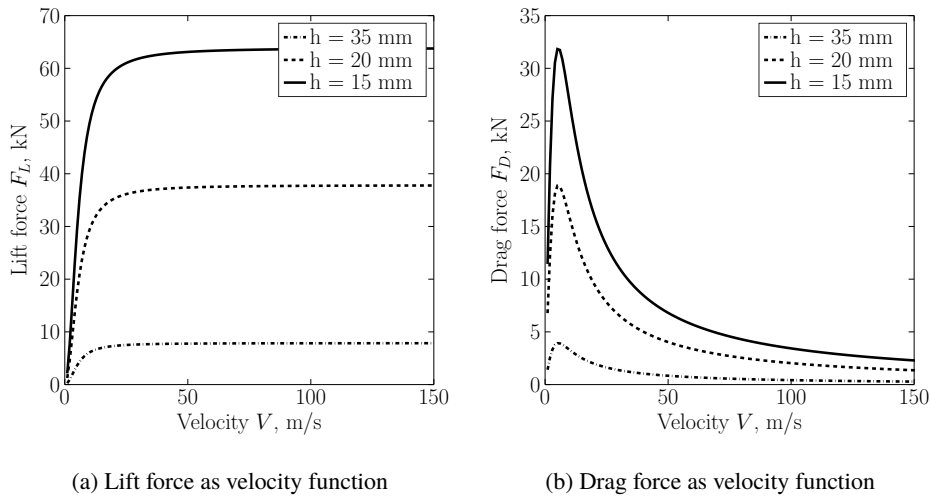
(b) Drag force as velocity function

Fig. 3. Lift (a) and drag (b) forces as velocity function for a constant air gap values

Please note that at high speeds the influence of velocity can be neglected, hence, motions in the horizontal and vertical direction are decoupled, which is proven below:

$$\frac{\partial \widetilde{F_L}(V_0, h_0)}{\partial V} = \Lambda_L e^{-\alpha h} \frac{\partial}{\partial V} \frac{V^2}{V^2 + \beta^2} = \Lambda_L e^{-\alpha h} \frac{2V\beta^2}{(V^2 + \beta^2)^2} \, . \tag{3}$$

For sufficiently small values of β and high velocity, part of the expression for the lift force (see Eq. (1a)) associated with velocity tends to a constant value of 1,

Natalia Strawa, Paweł Malczyk

which means that the function given in Eq. (3) tends to zero. Therefore, Eq. (2) can be reduced to the following expression:

$$\widetilde{F_L}(h) \cong \widetilde{F_L}(h_0) + \frac{\partial \widetilde{F_L}(h_0)}{\partial h} \Delta h. \tag{4}$$

Moreover, in the case of quarter suspension considered in this paper, an air gap h is expressed by two independent variables z_p and z_t. Thus, expression (4) can be written as:

$$\widetilde{F_L}(z_{p0}, z_{t0}) + \frac{\partial \widetilde{F_L}(z_{p0}, z_{t0})}{\partial z_p} \Delta z_p + \frac{\partial \widetilde{F_L}(z_{p0}, z_{t0})}{\partial z_t} \Delta z_t. \tag{5}$$

In the equilibrium point $z_{p0} = 0$ and $z_{t0} = 0$. Consequently, Eq. (5) transforms into:

$$\widetilde{F_L} \cong \widetilde{F_L}(0, 0) + \frac{\partial \widetilde{F_L}(0, 0)}{\partial z_p} z_p + \frac{\partial \widetilde{F_L}(0, 0)}{\partial z_t} z_t, \tag{6}$$

which yields:

$$\widetilde{F_L} \cong 0 - \Lambda_L \alpha e^{-\alpha \cdot h_0} z_p + \Lambda_L \alpha e^{-\alpha \cdot h_0} z_t. \tag{7}$$

The final formula for the linearized lift force is given as:

$$\widetilde{F_L} \cong -\Lambda_L \alpha e^{-\alpha \cdot h_0} (z_p - z_t). \tag{8}$$

By comparing expression (8) with the Hooke's law, one may observe that the linearized lift force can be represented as a "magnetic spring". Under the assumption that $k_m^* = \Lambda_L \alpha e^{-\alpha \cdot h_0}$, the orce generated by the "magnetic spring" is:

$$\widetilde{F_L} = -k_m^* (z_p - z_t). \tag{9}$$

Similar reasoning may be performed for the expression associated with the drag force. Such representation of the magnetic forces thoroughly simplifies the further analysis of the vehicle dynamic properties. Fig. 4 provides the relationship between air gap deviations from equilibrium and relative error of the linearized lift force. The results were obtained with the parameters presented in Table 1 and 2.
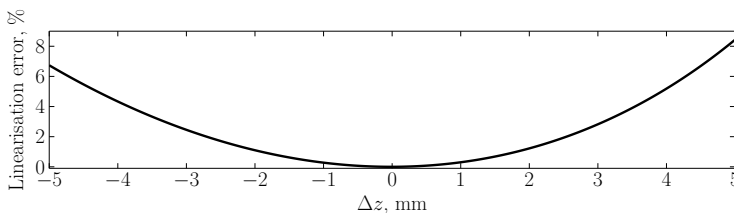

Fig. 4. Relative error of the linearized lift force

Table 2.

Suspension parameters

Parameter	Value	Unit
primary suspension mass, m_p	0.05×10^3	kg
secondary suspension mass, m_s	1.325×10^3	kg
secondary suspension stiffness, k_s	8.125×10^5	N/m
secondary suspension damping, b_s	5.040×10^4	Ns/m
magnetic levitation "stiffness", k_m^*	7.405×10^5	N/m

The final form of the equations of motion for the vehicle quarter-suspension model can be written in the following way:

$$m_p \ddot{z}_p = b_s(\dot{z}_s - \dot{z}_p) + k_s(z_s - zp) - k_m^*(z_p - zt), \tag{10a}$$

$$m_s \ddot{z}_s = -b_s(\dot{z}_s - \dot{z}_p) - k_s(z_s - z_p). \tag{10b}$$

Let us assume that s is the Laplace transform operator and $Z_p(s)$, $Z_s(s)$, $Z_t(s)$ are the Laplace transforms of $z_p(t)$, $z_s(t)$ and $z_t(t)$, respectively. The following transfer functions can be found from (10) by taking into account (9):

$$G_p(s) = \frac{Z_p(s)}{Z_t(s)} =$$
$$\frac{k_m^* \left(m_s s^2 + b_s s + k_s\right)}{m_p m_s s^4 + (m_p + m_s)b_s s^3 + \left[(m_p + m_s)k_s + k_m^* m_s\right] s^2 + k_m^* b_s s + k_m^* k_s}, \tag{11}$$

$$G_s(s) = \frac{Z_s(s)}{Z_t(s)} =$$
$$\frac{k_m^* \left(b_s s + k_s\right)}{m_p m_s s^4 + (m_p + m_s)b_s s^3 + \left[(m_p + m_s)k_s + k_m^* m_s\right] s^2 + k_m^* b_s s + k_m^* k_s}. \tag{12}$$

Now, the expressions (11) and (12) are exploited to build a block diagram of the passive suspension system, which is presented in Fig. 5.
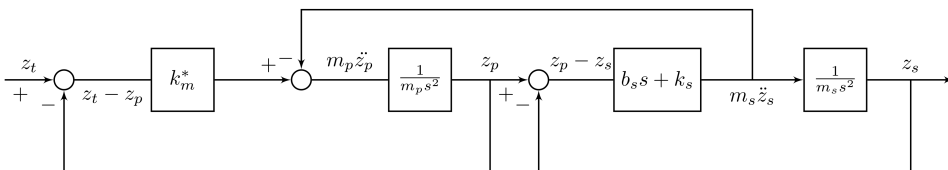

Fig. 5. Block diagram for two-degree-of-freedom suspension model

Please note that the upper branch of the block diagram indicates that the motion of the mass m_p is dependent on the motion of the mass m_s. This feature has some implications when control design is considered. The block diagram in Fig. 5 will be extensively used in subsequent chapters.

2.2. Transient response of suspension system

Transfer functions, introduced in Eq. (11) and Eq. (12), can be further utilised to obtain transient response of primary and secondary suspension. Fig. 6 shows the dynamic responses of the components when the system is triggered by unit-step input of signal associated with track perturbation. The results presented here and further in this paper were obtained with data provided in Table 2. It can be easily observed that secondary suspension has greater overshoot and its response is delayed with respect to a primary suspension.
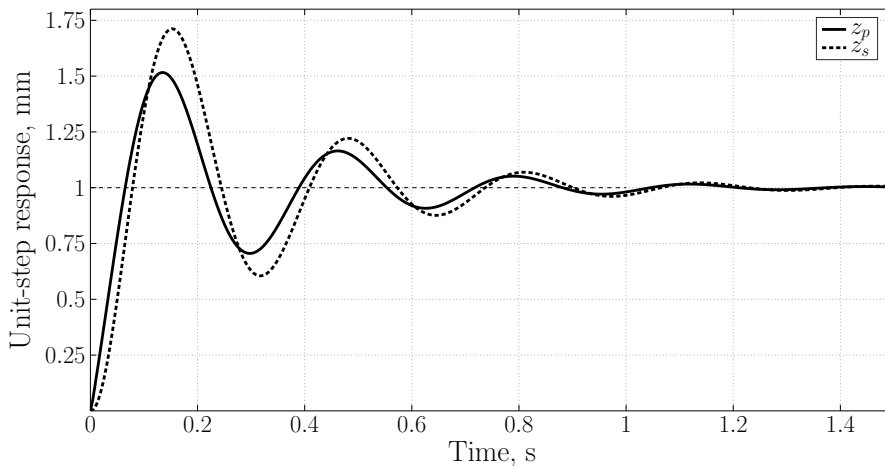

Fig. 6. Transient response of primary and secondary suspension with a unit-step input of track perturbation

2.3. Stability of passive suspension system

G_p and G_s have identical denominators, therefore, their respective eigenvalues – two real and two conjugated, i.e. $\lambda_{1,2} = -3.54 \pm 19.2j$, $\lambda_3 = -23.6$, $\lambda_4 = -1015.4$ – are the same.

Due to the control quality issues, damping ratio for a second-order system should be between 0.4 and 0.8 [5]. The damping ratio for the analyzed suspension is 0.182 and is below that range. It can be noted that all poles are placed in the left-half complex s-plane, thus, both open-loop systems are naturally stable. One real pole is placed far from the imaginary axis compared to the remaining eigenvalues,

which means that its influence on the system performance is minimal. Ultimately, the difference between G_p and G_s responses is associated with the numerator of each transfer function. G_p has two conjugated zeroes: $z_{1,2} = -19 \pm 15.9j$, while G_s has only one real zero: $z_1 = -16.1$.

It can be observed that there is no need for an active control system to provide stability. However, passengers' ride comfort requires substantial improvements. Hence, it is highly recommended to implement some kind of control system in order to enhance suspension performance.

Next, the system behaviour under uncertainties was investigated. We assumed that the actual values of the following parameters: mass of the primary suspension m_p, mass of the secondary suspension m_s and Halbach array parameter Λ_L may deviate from the nominal values used in this study by $\pm 20\%$. Secondary suspension response to the step input was obtained for the given range of parameters. It can be found in Fig. 7. One can notice that uncertainties do not cause unstable behaviour of the system. Various parameter values mainly influence time that the system needs to obtain the steady-state.
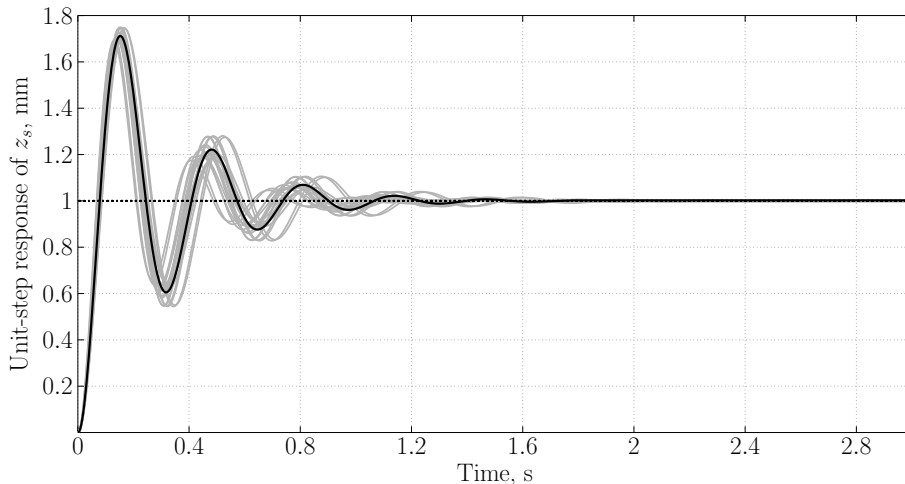

Fig. 7. Transient response of secondary suspension with uncertainties to a unit-step input of track perturbation

2.4. Three-degrees-of-freedom vehicle model

Three-degrees-of-freedom vehicle model is presented in Fig. 8. In this case, the vehicle can move in longitudinal x-direction and vertical z-direction. Simultaneously, it is able to rotate through a pitch angle θ about the z-axis. The model represents half of the vehicle with two independent suspension systems placed at the front and rear of the vehicle body. Therefore, the secondary suspension mass, which represents the mass of the main vehicle body, equals $m_s = 2.650 \times 10^3$ kg.

The rotational moment of inertia $I_\theta = 268.8\ \text{kg·m}^2$. Primary suspension parameters for each system are the same as for quarter-suspension model and were provided earlier in this paper in Table 2. The control system of the suspension is exactly the same as the one used for the quarter-suspension model.
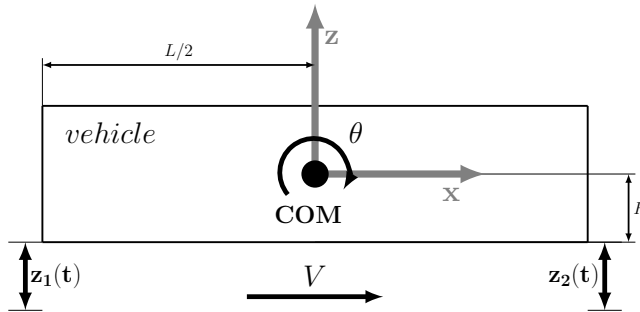

Fig. 8. Three-degree-of-freedom vehicle model

Equations of motion for 3-DOF vehicle moving at a velocity $V(t)$ at $z_1(t)$ and $z_2(t)$ levitation height can be formulated as [5, 15]:

$$m\ddot{X}(t) = P - F_{D1}(z_1, V, t) - F_{D2}(z_2, V, t),$$

$$\frac{m}{2}\left[\ddot{Z}_1(t) + \ddot{Z}_2(t)\right] = -mg + F_{L1}(z_1, V, t) + F_{L2}(z_2, V, t),$$

$$\frac{I_\theta}{L}\left[\ddot{Z}_1(t) - \ddot{Z}_2(t)\right] = \frac{L}{2}\left[F_{L1}(z_1, V, t) - F_{L2}(z_2, V, t)\right]$$
$$+ H\left[F_{D1}(z_1, V, t) + F_{D2}(z_2, V, t)\right], \tag{13}$$

where m is the vehicle mass, I_θ is the rotational moment of inertia about the y-axis of the vehicle centroidal frame, P is the propulsion force, F_{L1}, F_{L2} are the magnetic lift forces and F_{D1}, F_{D2} are the magnetic drag forces. Coordinates Z_1 and Z_2 denote the rear and front secondary suspension position along z-axis, respectively, while X is the vehicle COM position along x-axis. The vehicle should move in the vacuum. Therefore, the aerodynamic drag force is not taken into account because of its marginal influence on the system behaviour in the low-pressure conditions.

Linearized equations of motion for a 3-DOF vehicle moving at a velocity $V(t)$ at $z_1(t)$ and $z_2(t)$ levitation heights can be formulated as follows [13]:

$$m\ddot{X}(t) + K_{xz1}z_1 + K_{xz2}z_2 = 0,$$

$$\frac{m}{2}\left[\ddot{Z}_1(t) + \ddot{Z}_2(t)\right] + K_{zz1}z_1 + K_{zz2}z_2 = 0,$$

$$\frac{2I_\theta}{L^2}\left[\ddot{Z}_1(t) - \ddot{Z}_2(t)\right] - K_{zz1}z_1 + K_{zz2}z_2 = 0, \tag{14}$$

where K_{xz1}, K_{xz2}, K_{zz1}, K_{zz2} are partial derivatives of lift and drag forces with respect to the vehicle position defined as follows:

$$K_{xzi} = \frac{\partial F_{Di}}{\partial z_i} \qquad K_{zzi} = \frac{\partial F_{Li}}{\partial z_i}, \qquad i = 1, 2. \tag{15}$$

Note that the drag force disappeared from the torque equation in (14). Such a simplification can be made because partial derivatives of the drag force are approximately zero at high speeds and have little influence on the vehicle rotational dynamics when compared to the lift force.

A 3-DOF vehicle model was employed in a series of simulations presented further in this paper.

3. Control system design

In the suspension system control design process, several goals can be distinguished, e.g., passenger comfort, road handling, etc. Optimized suspension should be able to meet all those objectives, however, usually one of them is of the greatest weight. In this study, passenger ride comfort was chosen as the dominant target.

Track roughness induces random vibrations which are perceived by the passengers. Vibrations can cause many physiological effects, hence, ride quality is a serious constraint in suspension system design. Identification of the perception levels of the human body is based on experimental data. Results obtained in multiple studies prove that the critical range of whole-body vibration depends on organs resonant frequencies which could be placed between 1 and 20 Hz [6]. Passenger ride comfort can be quantitatively measured by the acceleration output power spectral density (PSD) of the secondary suspension [6].

Assuming that V is the vehicle velocity, A is the roughness amplitude and ω is the disturbance frequency, surface roughness of the track can be approximated by the PSD of surface profile:

$$S(\omega) = \frac{AV}{\omega} . \tag{16}$$

Then, the acceleration output PSD is defined as [14]:

$$\Phi(\omega) = AV|j\omega \cdot G_s(j\omega)|^2 \cdot \frac{2\pi}{g} \ [\text{Hz}], \tag{17}$$

where g is the gravitational acceleration and multiplication by 2π converts the result to per-Hertz basis.

Nowadays, for the evaluation of ride comfort a guideline proposed by the US Department of Transportation is widely used. It is known as Urban Tracked Aircushion Vehicle (UTACV) criterion [6]. This criterion has been established after conducting an extensive experimental research on the influence of the certain

vibration frequencies on a human body. The criterion restricts the maximum value of PSD in the given frequency spectrum that can be reached in the vehicle while transporting people.

3.1. Active control of a primary suspension

The first concept for ride comfort improvement is an implementation of active control in a primary suspension system. This could be realized by adding an electro-pneumatic or electro-hydraulic actuator between the package of levitation magnets and a primary suspension module (see Fig. 9a). Such a system would provide a constant air gap between magnets and track as well as attenuate oscillations, which should result in enhanced ride comfort.

(a) Active control system, primary
suspension

(b) Semi-active control for secondary
suspension
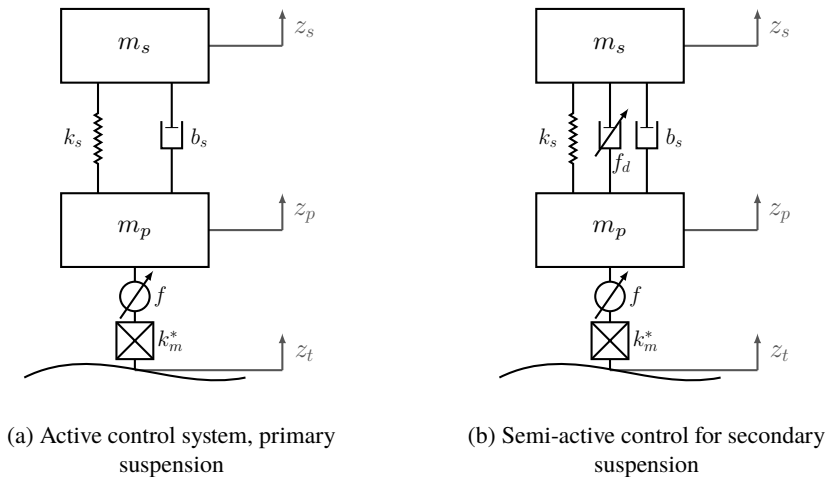
Fig. 9. Control system schematics for vehicle suspension

Among multiple control system design architectures, the one with a controller in inner feedback path was chosen by taking into account that acceleration feedback gain can modify both the natural frequency and damping of the suspension while the position feedback gain can modify nothing but the natural frequency [5, 6, 15]. The controller is placed so that its reference input signal is a primary suspension displacement whilst output is proportional to the force generated by an actuator (see Fig. 13). Note that acceleration of primary suspension is naturally dependent on the acceleration of secondary suspension. Consequently, the control feedback loop input signal is proportional to the lift force and the forces transmitted through the spring and damper. Lead compensator was chosen for a primary suspension control unit with coefficients found by means of the loop shaping method [16].

The main goal of the loop-shaping method is to find controller parameters that provide the desired shape of an open-loop system with proper disturbance rejection and noise attenuation [16]. For the suspension system, the loop of interest is the

main (outer) feedback loop while the controller itself is placed in the feedback path of the inner loop. Consequently, expressions for transfer functions used in the loop-shaping method become fairly complicated if delivered explicitly with the controller transfer function. To make the problem more transparent, the whole feedback inner loop will be represented as C_1. It can be assumed that in the considered case, the reference signal always equals zero as we want to maintain constant levitation height. The graphical representation of the described system can be found in Fig. 10.
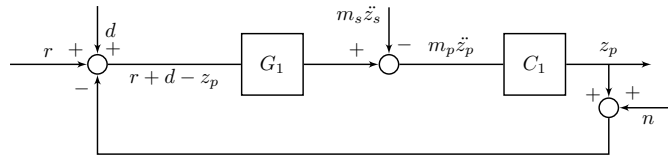
Fig. 10. Primary suspension control design block diagram

The following notation is assumed: $G_1 = k_m^*$ – transfer function of primary suspension forward path from input r to $m_p \ddot{z}_p$ and C_1 – transfer function of the inner feedback loop. Moreover, r is a reference signal, d – track disturbances, n – sensor measurement noise and d_s – disturbances from secondary suspension coupling $m_s \ddot{z}_s$.

Therefore, expression for an output signal $Z_p(s)$ can be obtained as:

$$Z_p(s) = \underbrace{\frac{G_1 C_1}{1 + G_1 C_1}}_{T} r + \frac{G_1 C_1}{1 + G_1 C_1} d - C_1 \underbrace{\frac{1}{1 + G_1 C_1}}_{S} d_s - \frac{G_1 C_1}{1 + G_1 C_1} n. \qquad (18)$$

Function T is a complementary sensitivity function while S is a sensitivity function [16]. Moreover, an open-loop transfer function is defined as: $L = G_1 C_1$. Assuming that the reference signal r is zero, the output signal $Z_p(s)$ can be written as:

$$Z_p(s) = Td - C_1 S d_s - Tn. \qquad (19)$$

It can be observed that complementary sensitivity function should have low values for the frequencies where disturbances and noises are expected. Controller parameters obtained with loop-shaping method yields the results presented in Fig. 11 and Fig. 12.

The final values for the controller parameters are shown in Table 3, where the lead compensator is given by:

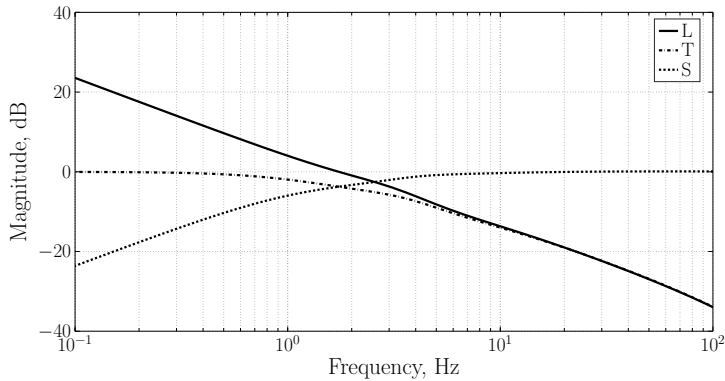$$K_{lead} = K_c \frac{s + a_{lead}}{s + b_{lead}}. \qquad (20)$$

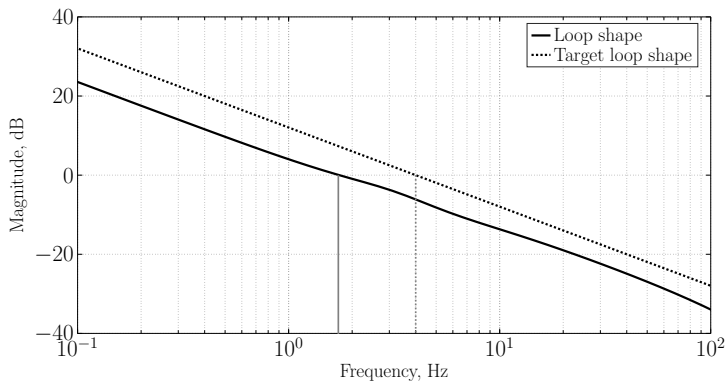Fig. 11. Sensitivity, complementary sensitivity and open-loop system magnitude plots

Fig. 12. Loop shape goal vs. actual loop shape for primary suspension control design

Table 3.

Lead compensator parameters

Parameter	Value
K_c	1.887×10^6
a_{lead}	0.0095
b_{lead}	24.1

3.2. Semi-active control of secondary suspension

Secondary suspension performance can be improved by introduction of semi-active control, i.e., damper with adjustable viscous damping coefficient used in parallel with passive spring [5]. The proposed system is illustrated in Fig. 9b.

Again, similarly to active control in primary suspension, a controller is implemented in the inner feedback path. This time, displacement of secondary suspension bogie is taken for an input reference value whilst the controller output is proportional to the damping force of active damper. In this case, PD controller was chosen

and its parameters were obtained with the loop-shaping approach similar to that presented in the previous section. Block diagram of the suspension system with both active and semi-active control is provided in Fig. 13. Transient response of the secondary part of the suspension for a unit-step input of 1 mm track perturbation is depicted in Fig. 14 for various control systems involved in the solution.
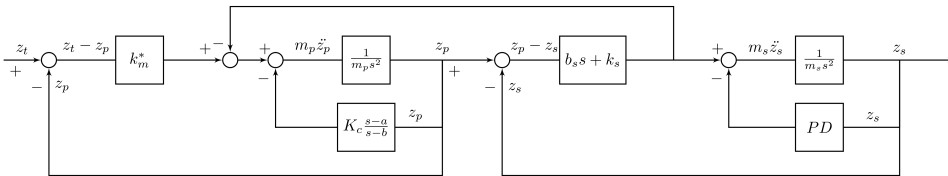

Fig. 13. Block diagram for suspension model with active control in primary suspension and semi-active control in secondary suspension
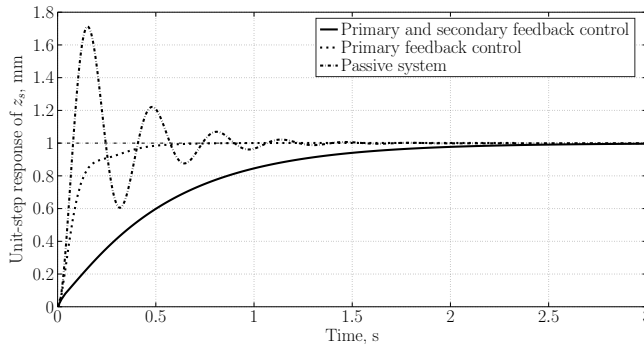
Fig. 14. Transient response of secondary suspension

Please note that the response of the system due to track irregularity is oscillatory for a passive system. Nevertheless, the proposed control scheme allows attenuating the vibrations to provide an overdamped step response at a price of additional control systems implemented on-board the vehicle. The tuned gains of the PD controller can be found in Table 4. Note that T_f is the time constant of the first-order derivative filter.

Table 4.
PD controller gains

Parameter	Value
K_P	510
K_D	7×10^5
T_f	0.004

Finally, robustness of the control system was analysed. The quarter-suspension response to the unit-step input perturbation was investigated for the uncertain model introduced in Section 2.3. Results for both control schemes described above are presented in Fig. 15. It can be concluded that the uncertainties do not have any negative influence on the control performance.
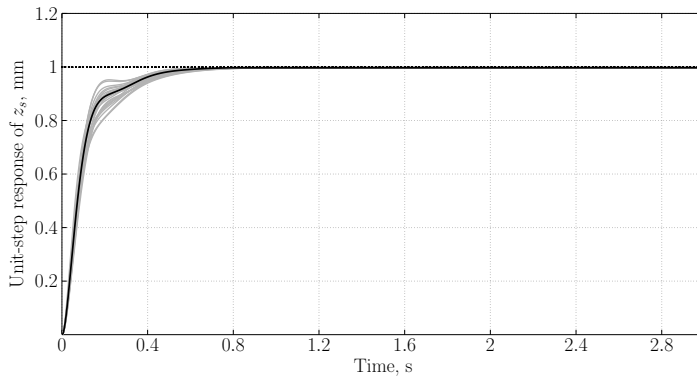
(a) With active control in primary suspension
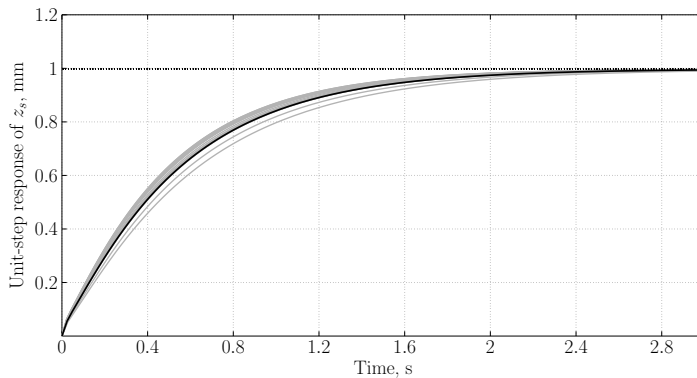
(b) With active control in primary suspension and semi-active control
in secondary suspension

Fig. 15. Transient response of secondary suspension with uncertainties to a unit-step input
of track perturbation

In order to evaluate passengers' ride comfort, the ride comfort criterion has been chosen [6], which was specifically defined for Maglev trains. As can be observed in Fig. 16, despite the significant decrease in acceleration output power spectral density (PSD) for an active system, the criterion is still exceeded but it is nicely met for the frequencies up to 4 Hz. Further work is needed in this regard.
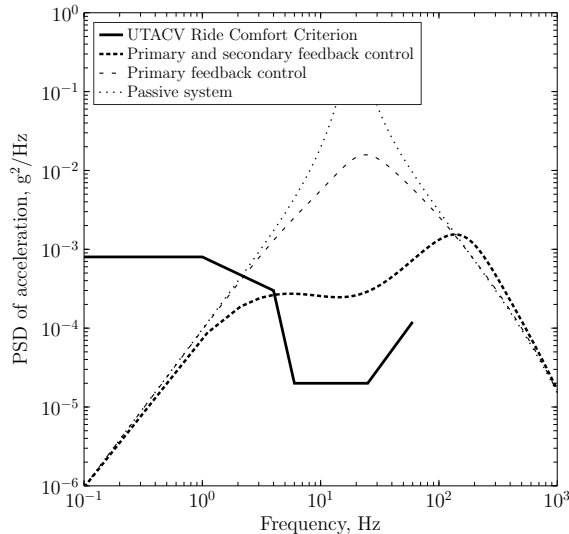
Fig. 16. PSD of secondary suspension acceleration, velocity $V = 150$ m/s,
track roughness amplitude $A = 10^{-6}$ m

4. Simulation results

A number of simulation scenarios were implemented for quarter suspension and planar 3-DOF system. The simulations were run in the Matlab/Simulink environment. A variable-step Dormand-Prince (ode45) solver was used.

First, let us consider a one-dimensional system. A 5 mm half-period sine bump was chosen as an input signal in the first test case. Disturbances of such a large amplitude are not expected to occur in real track conditions, however, in this study, such irregularities can be considered as a worst-case scenario. Parameters of the suspension system assumed for the analysis are presented in Table 2. Moreover, we assume that the vehicle travels at the speed of $V = 150$ m/s.

It can be noticed (see Fig. 17) that for passive system bump amplitude is amplified, resulting in an excessive displacement of a vehicle bogie which is inherently connected with a high value of acceleration output. When active control in a primary suspension is implemented, the influence of the bump is much smaller from the perspective of passengers' disturbance perception.

Much more satisfactory results are obtained for a suspension with feedback control in the primary and secondary system implemented simultaneously. In this case, displacement of the upper part of the suspension is negligible compared to the bump amplitude.

In the next test case, a white noise signal simulating track surface roughness was implemented. Similarly to the previously discussed example, peak noise amplitude of 1 mm is excessively bigger than actual roughness of the aluminium plates used in the track construction.
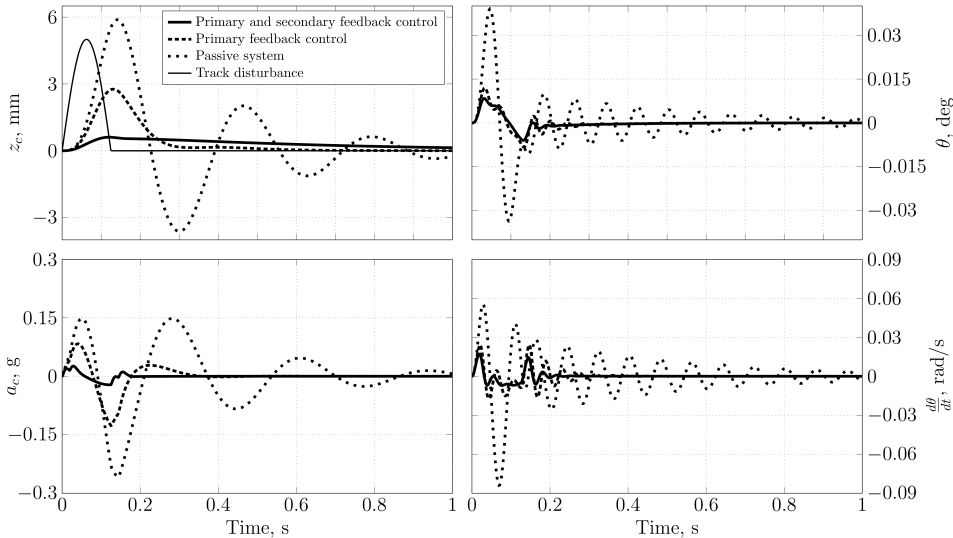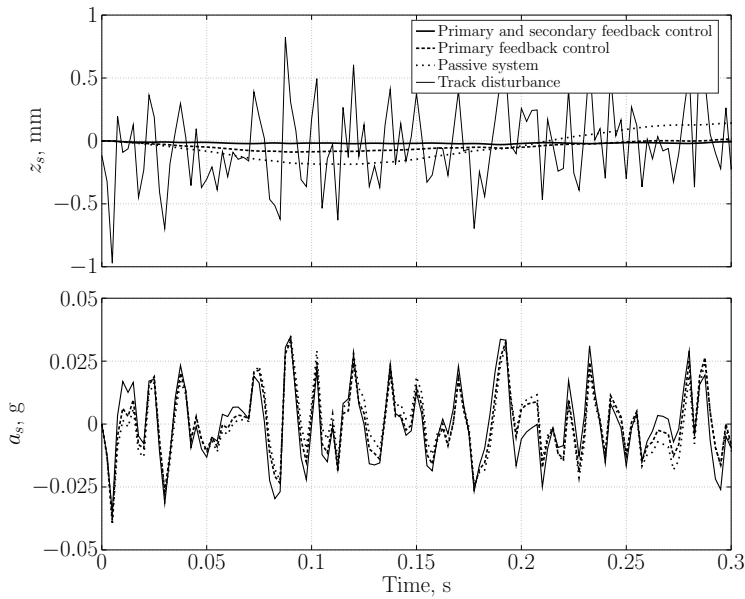
Fig. 17. Quarter-suspension response to sinusoidal bump track disturbance

The most straightforward observation from suspension performance analysis in a vibrational environment is that hybrid active and semi-active suspension system displacement is much smaller than input signal amplitude. At the same time, passive suspension displacement can be approximated by a sinusoidal wave of the 0.4 s period, which may not be visible in Fig. 18a due to the scale used in the graph. On the other hand, acceleration output is small for all suspension configurations.

The last simulation scenario of the quarter-suspension system aimed at investigating how the developed control schemes perform when the non-linear suspension model is considered. The secondary suspension displacement of the non-linear model is compared with the response of linearized suspension in Fig. 19. One can observe that the secondary suspension displacement of the non-linear model has slightly bigger amplitude. Nonetheless, it can be concluded that there are minor differences in the performance of both control approaches between linearized and non-linear models.

Similarly to the one-dimensional case, a 3-DOF model response for a sinusoidal bump was investigated and presented in Fig. 20. Pitch angle reaches marginally small values below 0.04$^\mathrm{o}$ for passive system and below 0.01$^\mathrm{o}$ for active and active plus semi-active configuration. With the action of the controllers employed, the system is stabilized very quickly; after approx. 0.2 s, the pitch angle is reduced to zero.

The last test case is considered in order to evaluate the vehicle response to the input signals which possess diverse frequency content. Two sinusoidal input

(a) Secondary suspension displacement and acceleration
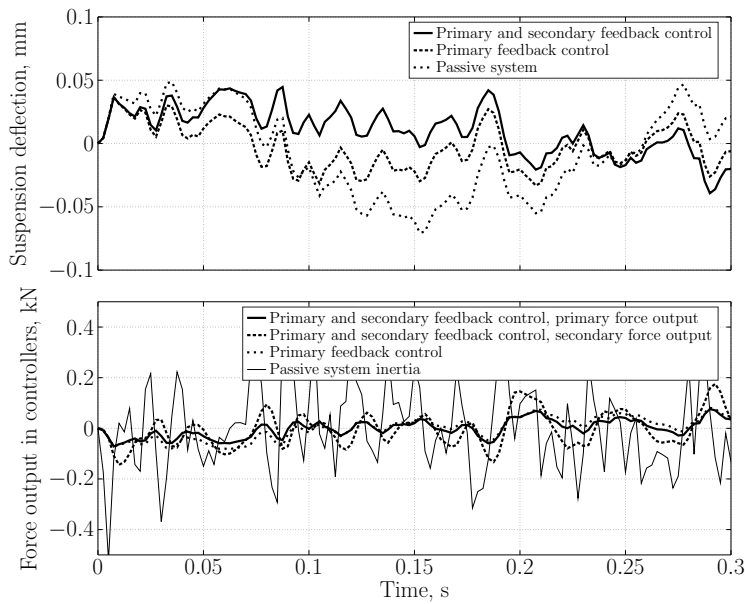
(b) Suspension deflection and feedback force of active elements
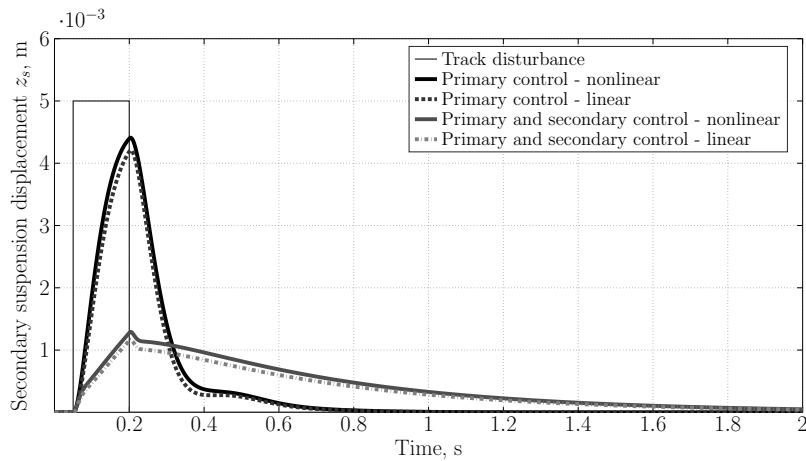
Fig. 18. Suspension response to track roughness

Fig. 19. Comparison of the non-linear and linearized quarter-suspension response
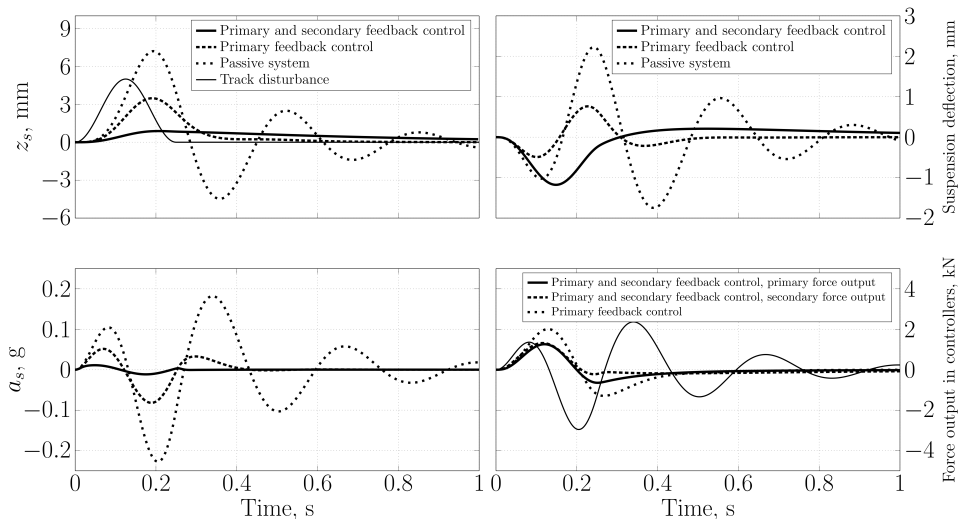to the track disturbance

Fig. 20. 3-DOF suspension response to sinusoidal bump track disturbance

signals were defined: a sine wave of frequency of 0.05 Hz and an amplitude of
2 mm together with a sine wave of 9 Hz frequency and 1 mm amplitude. The
sample numerical results of the simulations are presented in Fig. 21. It can be
observed that the vehicle pitch angle is proportional to the track slope, while high-
frequency low-amplitude oscillations are induced due to the track roughness. The
most important conclusion is that the vehicle remains stable when influenced by
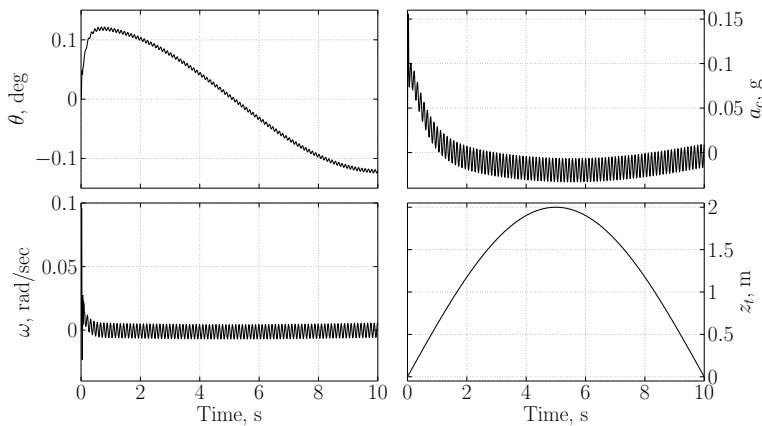the combined signals of high and low frequencies.

Fig. 21. 3-DOF vehicle response to low frequency changes of track topography
and high frequency disturbances

5. Discussion and conclusions

The main aim of the study described in this paper was to develop a simplified model of the system and analyze the dynamic performance of a preliminary concept of a high-speed vehicle suspension system with particular emphasis on passengers' ride comfort. Moreover, a methodology for control system design was proposed in order to improve ride stability and comfort by adopting a frequency-based loop shaping method.

First important finding is that electrodynamic suspension in the vehicle guarantees stability without the support of any active control system. Nonetheless, the dynamic response of the vehicle has a highly oscillatory character which, in consequence, results in high vertical acceleration values and implies poor ride comfort quality. Hence, the application of an active control system, which would properly compensate track disturbances, is highly recommended.

Implementation of the active element in a primary suspension system clearly improves its performance reducing oscillations about equilibrium point and extensive overshoot of system response due to a unit-step input. Simultaneously, the ride comfort is slightly enhanced this way. On the other hand, semi-active control of secondary suspension improves ride comfort considerably. Regardless of the selected control system configuration, the UTACV criterion is met up to 4 Hz but slightly exceeded for higher frequencies. Sensitivity analysis and overall optimization of vehicle dynamics and ride comfort through the use of generalized optimization techniques, such as the adjoint-based methods [17, 18], might be a solution to improve the results in this case. Further research is needed in modelling and control design of a system in order to gain understanding of dynamic performance of the vehicle under varying conditions.

Acknowledgements

References

[1] E. Musk. *Hyperloop Alpha*. Technical Report. Space Exploration Technologies Corporation, 2013.

[2] R.F. Post and D. Ryutov. *The Inductrack: a new approach to magnetic levitation*. Technical Report. Lawrence Livermore National Laboratory, USA, 1996. doi: 10.2172/237425.

[3] A.A. Shabana, K.E. Zaazaa, and H. Sugiyama. *Railroad Vehicle Dynamics: A Computational Approach*. CRC Press, 2007.

[4] Z. Liu, Z. Long, and X. Li. *Maglev Trains. Key Underlying Technologies*. Part of the Springer *Tracts in Mechanical Engineering* book series, Springer, 2015. doi: 10.1007/978-3-662-45673-6_1.

[5] Y. Cai, S.S. Chen, and D.M. Rote. Dynamics and controls in maglev systems. Technical Report, Argonne National Laboratory, USA, 1992. doi: 10.2172/10136539.

[6] P.K. Sinha. *Electromagnetic Suspension Dynamics and Control*. Peter Peregrinus Ltd., London, UK, 1987.

[7] M. Appleyard and P.E. Wellstead. Active suspensions: some background. *IEE Proceedings – Control Theory and Applications*, 142(2):123–128, 1995. doi: 10.1049/ip-cta:19951735.

[8] K.D. Rao. Modeling, simulation and control of semi active suspension system for automobiles under MATLAB Simulink using PID controller. *IFAC Proceedings Volumes*, 47(1):827–831, 2014. doi: 10.3182/20140313-3-IN-3024.00094.

[9] D. Hanafi. PID controller design for semi-active car suspension based on model from intelligent system identification. In: *2010 Second International Conference on Computer Engineering and Applications*, volume 2, pages 60–63, Bali Island, Indonesia, 19-21 March 2010. doi: 10.1109/ICCEA.2010.168.

[10] M. Sentil Kumar. Development of active suspension system for automobiles using PID controller. *Proceedings of the World Congress on Engineering 2008*, volume II, pages 1472–1477, London, UK, 2-4 July, 2008.

[11] A.J. Truscott and P.E. Wellstead. Adaptive ride control in active suspension systems. *Vehicle System Dynamics*, 24(3):197–230, 1995. doi: 10.1080/00423119508969088.

[12] U.N.L.T. Alves, J.P.F. Garcia, M.C.M. Teixeira, S.C. Garcia, and F.B. Rodrigues. Sliding mode control for active suspension system with data acquisition delay. *Mathematical Problems in Engineering* 2014:1-13, 2014. doi: 10.1155/2014/529293.

[13] Y. Cai, S.S. Chen, T.M. Mulcahy, and D.M. Rote. Dynamic stability of maglev systems. Technical Report, Argonne National Laboratory, USA, 1992. doi: 10.2172/10110331.

[14] R.M. Katz, V.D. Nene, R.J. Ravera, and C.A. Skalski. Performance of magnetic suspensions for high speed vehicles operating over flexible guideways. *Journal of Dynamic Systems, Measurement, and Control*, 96(2):204–212. doi: 10.1115/1.3426792.

[15] W. Kortüm, W. Schwartz, and I. Fayé. Dynamic modeling of high speed ground transportation vehicles for control design and performance evaluation. In: Schweitzer G., Mansour M. (eds), *Dynamics of Controlled Mechanical Systems. Proceedings of IUTAM/IFAC Symposium*, pages 335–350, Zurich, Switzerland, May 30–June 3, 1988. doi: 10.1007/978-3-642-83581-0_26.

[16] K.J. Aström and R.M. Murray. *Feedback Systems: An Introduction for Scientists and Engineers*. Princeton University Press, USA, 2008.

[17] P. Maciąg, P. Malczyk, and J. Frączek. Optimal design of multibody systems using the adjoint method. In: Awrejcewicz J. (ed.), *Dynamical Systems in Applications*, pages 240–253. Springer, 2018. doi: 10.1007/978-3-319-96601-4_22.

[18] Y. Zhu, C. Sandu, D. Dopico, and A. Sandu. Benchmarking of adjoint sensitivity-based optimization techniques using a vehicle ride case study. *Mechanics Based Design of Structures and Machines*, 46(2):254–266, 2018. doi: 10.1080/15397734.2017.1338576.